LA-UR-14-20244
Approved for public release; distribution is unlimited.

Title: Geometrically induced surface polaritons in planar nanostructured metallic cavities"

Author(s): Davids, P. S.
Intravia, F
Dalvit, Diego A.

Intended for: Optics Express

Issued: 2014-01-14

Geometrically induced surface polaritons in planar nanostructured metallic cavities

P. S. Davids[1], F. Intravaia[2], D.A.R. Dalvit[2]

[1]*Applied Photonics and Microsystems, Sandia National Laboratories, Albuquerque, NM 87185, USA*
[2]*Theoretical Division, MS B213, Los Alamos National Laboratory, Los Alamos, NM 87545, USA*

Abstract: We examine the modal structure and dispersion of periodically nanostructured planar metallic cavities within the scattering matrix formulation. By nanostructuring a metallic grating in a planar cavity, artificial surface excitations or spoof plasmon modes are induced with dispersion determined by the periodicity and geometric characteristics of the grating. These spoof surface plasmon modes are shown to give rise to new cavity polaritonic modes at short mirror separations that modify the density of modes in nanostructured cavities. The increased modal density of states from the cavity polaritons have a large impact on the fluctuation induced electromagnetic forces and enhanced heat transfer at short separations.

OCIS codes: (000.0000) General.

References and links

1. A. Castanié and D. Felbacq, "Confined plasmonic modes in a nanocavity," Optics Communications **285**, 3353–3357 (2012).
2. Y. Kurokawa and H. Miyazaki, "Metal-insulator-metal plasmon nanocavities: Analysis of optical properties," Physical Review B **75**, 1–13 (2007).
3. B. Sturman, E. Podivilov, and M. Gorkunov, "Eigenmodes for metal-dielectric light-transmitting nanostructures," Physical Review B **76**, 125104 (2007).
4. G. Sun, J. B. Khurgin, and D. P. Tsai, "Spoof plasmon waveguide enabled ultrathin room temperature thz gan quantum cascade laser: a feasibility study," Optics Express **21**, 28054–28061 (2013).
5. J. B. Pendry, L. Martín-Moreno, and F. J. Garcia-Vidal, "Mimicking surface plasmons with structured surfaces," Science (New York, N.Y.) **305**, 847–8 (2004).
6. F. J. Garcia-Vidal, L. Martín-Moreno, and J. B. Pendry, "Surfaces with holes in them: new plasmonic metamaterials," Journal of Optics A: Pure and Applied Optics **7**, S97–S101 (2005).
7. D. W. Peters, P. Davids, J. R. Wendt, A. a. Cruz-Cabrera, S. a. Kemme, and S. Samora, "Metamaterial-inspired high-absorption surfaces for thermal infrared applications," Library **7609**, 76091C–76091C–7 (2010).
8. D. W. Peters, C. M. Reinke, P. S. Davids, J. F. Klem, D. Leonhardt, J. R. Wendt, J. K. Kim, and S. Samora, "Nanoantenna-enabled midwave infrared focal plane arrays," **8353**, 83533B–83533B–6 (2012).
9. G. Bimonte, "Scattering approach to casimir forces and radiative heat transfer for nanostructured surfaces out of thermal equilibrium," Physical Review A **80**, 042102 (2009).
10. P. S. Davids, F. Intravaia, F. D. S. S. Rosa, and D. Dalvit, "Modal approach to Casimir forces in periodic structures," Physical Review A **82**, 1–12 (2010).
11. A. Lambrecht and V. Marachevsky, "Casimir Interaction of Dielectric Gratings," Physical Review Letters **101**, 1–4 (2008).
12. J. Lussange, R. Guérout, F. S. S. Rosa, J.-J. Greffet, a. Lambrecht, and S. Reynaud, "Radiative heat transfer between two dielectric nanogratings in the scattering approach," Physical Review B **86**, 085432 (2012).
13. M. T. H. Reid, J. White, and S. G. Johnson, "Fluctuating surface currents: An algorithm for efficient prediction of Casimir interactions among arbitrary materials in arbitrary geometries," Physical Review A **88**, 022514 (2013).

14. A. W. Rodriguez, F. Capasso, and S. G. Johnson, "The casimir effect in microstructured geometries," Nature photonics **5**, 211–221 (2011).
15. F. Intravaia, S. Koev, I. W. Jung, a. A. Talin, P. S. Davids, R. S. Decca, V. a. Aksyuk, D. a. R. Dalvit, and D. López, "Strong Casimir force reduction through metallic surface nanostructuring," Nature communications **4**, 2515 (2013).
16. S.-a. Biehs, F. S. S. Rosa, and P. Ben-Abdallah, "Modulation of near-field heat transfer between two gratings," Applied Physics Letters **98**, 243102 (2011).
17. R. Carminati and J.-J. Greffet, "Near-field effects in spatial coherence of thermal sources," Physical Review Letters **82**, 1660 (1999).
18. A. Narayanaswamy, S. Shen, and G. Chen, "Near-field radiative heat transfer between a sphere and a substrate," Physical Review B **78**, 1–4 (2008).
19. A. Narayanaswamy, S. Shen, L. Hu, X. Chen, and G. Chen, "Breakdown of the Planck blackbody radiation law at nanoscale gaps," Applied Physics A **96**, 357–362 (2009).
20. R. Ottens, V. Quetschke, S. Wise, a. Alemi, R. Lundock, G. Mueller, D. Reitze, D. Tanner, and B. Whiting, "Near-Field Radiative Heat Transfer between Macroscopic Planar Surfaces," Physical Review Letters **107**, 1–4 (2011).
21. T. Jiang, L. Shen, X. Zhang, and L. Ran, "High-order modes of spoof surface plasmon polaritons on periodically corrugated metal surfaces," Progress In Electromagnetics Research , , **8**, 91–102 (2009).
22. L. Li, "Use of Fourier series in the analysis of discontinuous periodic structures," JOSA A **13**, 1870–1876 (1996).
23. L. Li, "Formulation and comparison of two recursive matrix algorithms for modeling layered diffraction gratings," JOSA A **13**, 1024–1035 (1996).
24. L. Li, "New formulation of the Fourier modal method for crossed surface-relief gratings," Journal of the Optical Society of America A **14**, 2758 (1997).
25. Z.-Y. Li and K.-M. Ho, "Analytic modal solution to light propagation through layer-by-layer metallic photonic crystals," Physical Review B **67**, 1–15 (2003).
26. Z.-Y. Li and L.-L. Lin, "Photonic band structures solved by a plane-wave-based transfer-matrix method," Physical Review E **67**, 1–11 (2003).

1. Introduction

Eigenmodes in planar metal insulator metal cavities at short separations have been extensively studied owing to the existence of surface plasmon excitations [1, 2, 3]. Surface plasmons are resonant optical excitations at metal dielectric interfaces and mainly arise due to the material dispersion of the metallic permittivity. These surface bound optical eigenmodes confine light to extreme sub-wavelength dimensions and many applications require extending surface plasmon confinement and dispersion to the infrared and THz parts of the electromagnetic spectrum [4]. Recently, Pendry and co-workers[5, 6] have proposed and demonstrated engineered dispersion by periodically nanostructuring surfaces by perforating perfect electrical conductors. It has been shown that these perforated nanostructured surfaces support surface modes that have dispersion similiar to real surface plasmons in metals, but with the effective plasma frequency determined by geometric parameters of the perforation. These engineered dispersive surface modes confine light to subwavelength regions and are called spoof surface plasmons. In a cavity configuration consisting of a two dimensional periodic frequency selective surface above a metallic ground plane, these geometrically induced surface modes give rise to perfect infrared absorbers which are actively under development for infrared filtering and detection applications[7, 8]. Furthermore, periodically nanostrutured cavities with strong confinement have been examined for THz quantum cascade laser applications[4] .

Recently, modal expansion techniques within the scattering approach have been used to examine fluctuation induced electromagnetic forces and energy transfer in nanostructured cavities[9, 10, 11, 12]. These cavities are separated by vacuum gaps or dielectric material and formed between a planar metallic mirror and a nanostructured grating. Finite temperature equilibrium electromagnetic forces in these planar cavities arise due to thermal or vacuum induced fluctuating currents on the cavity mirrors and their associated fluctuating electromagnetic fields[13]. By controlling the cavity modal dispersion and density of modes through periodic nanoscale structuring[14], one can modify the equilibrium cavity forces. Well known

geometric force approximations based on the decomposition of a complex structured surface into plane-plane segments with well defined integrated forces, known as the proximity force approximation (PFA), have been shown to break down at short cavity mirror separations resulting in enhanced attraction over these geometrically predicted forces[15].

In planar cavities driven out of thermal equilibrium, such as cavity mirrors with finite temperature differences maintained between the mirrors, nanostructured control of the cavity modes allows for tailored energy transfer from the hot surface to the cold surface. The modal structure of nonequilibrium cavities at separations shorter than the thermal wavelength leads to near-field heat transfer where evanescent surface modes on the planar surfaces at different temperatures can dominate the heat transfer [16, 17, 18, 19]. Nanostructuring of these surfaces can be used to tailor and enhance the heat transfer through design of the cavity modes which evanescently couple one surface to the other[12] for vacuum gaps much smaller than the thermal wavelength. This enhanced heat transfer has been experimentally measured in a planar cavity configuration and the enhanced near-field transfer at separations shorter than the thermal wavelength demonstrated[20].

The paper is organized as follows: In section II, we examine geometrically induced surface plasmon mode dispersion on a perfectly conducting metallic grating. In section III, the cavity modes in a planar nanostructured cavity are examined by modal expansion in the vacuum region between the two planar mirrors. The scattered fields from the metallic planar grating are treated using the Fourier modal scattering matrix method (RCWA) described in references [10]. The metallic cavity is assumed to be Au for both planar and nanostructured mirrors and the Drude model is used for the metallic dielectric permittivity in the cavity modal calculations. The modal expansion of the transverse fields in the planar cavity is performed and the cavity boundary value problem is treated in the vacuum region between the nanostructured surface and the planar mirror. A secular determinant for the cavity modal resonances is obtained from the boundary conditions. The relationship between the cavity modal density and energy density in terms of the secular determinant is derived. In section IV, the cavity modal dispersion is examined for varying mirror grating separation and new cavity polaritons related to the spoof plasmons on the nanostructured grating at short separations are observed. These new cavity polaritons increase the density of modes at the effective plasmon wavelength and give rise to an enhanced attractive forces at short separations. The modal dispersion is compared for nanostructured grating and planar unstructured mirror cavities.

2. Spoof surface modes

The simplest structure in which to examine these designer spoof surface plasmon modes is a perfectly conducting grating structure. Figure 1 shows schematically the basic 1D grating. We begin by considering the TM surface modes in the perfectly conducting grating structure with period L_x, with a groove of width w, and depth h. The electromagnetic boundary value problem is split into two regions. In region I, the vacuum or dielectric region above the etched grating, $z \leq 0$, the H field is given by Bloch mode expansion,

$$H_y^I = \sum_n H_n \exp(ik_x^{(n)} x - iq_z^{(n)} z), \tag{1}$$

where $k_x^{(n)} = k_x + 2\pi n/L_x$, and $q_z^{(n)} = \sqrt{k^2 - k_x^{(n)2}}$. The H field is over the entire period of the grating and satisfies Bloch periodic boundary conditions. The E field is obtained directly from Maxwells equations. The transverse electric field in region I is

$$E_x^I = -\sum_n \frac{q_z^{(n)}}{k} H_n \exp(ik_x^{(n)} x - iq_z^{(n)} z). \tag{2}$$

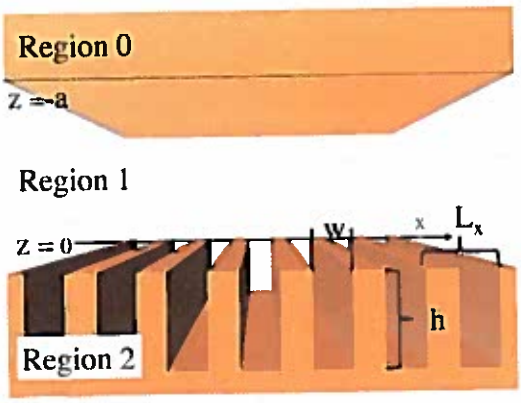

Fig. 1. Grating mirror based cavity examined. The lower mirror is a periodically structured metallic grating. The upper mirror is a metallic plane.

Region II is defined for $z \geq 0$, the groove is etched in a perfect conductor, thus the electric field is confined in the groove, ($|x| \leq w/2$), and must vanish at the bottom of the groove. The electric field is given by

$$E_x^{II} = B\sin(k(z-h)) \tag{3}$$

and $E_z^{II} = 0$. The transverse magnetic field in the groove is

$$H_y^{II} = -iB\cos(k(z-h)). \tag{4}$$

The boundary conditions at the grating top surface, $z = 0$, require the continuity of the tangential H fields. By integrating over the groove width we obtain

$$\sum_n H_n s_n = -iB\cos(kh), \tag{5}$$

where

$$s_n = \frac{\sin\left(k_x^{(n)} w/2\right)}{k_x^{(n)} w/2}. \tag{6}$$

The continuity of the tangential electric field at $z = 0$ and using the orthogonality of the Fourier mode expansion, we obtain

$$H_n = B\frac{k}{q_z^{(n)}}\frac{w}{L_x}\sin(kh)s_n^2. \tag{7}$$

Combining Eq. (5) and Eq.(7), we obtain the resonance condition for the spoof surface plasmons,

$$\frac{kw}{L_x}\sum_n \frac{s_n^2}{\sqrt{k_x^{(n)2} - k^2}} = \cot(kh), \tag{8}$$

for the multimodal single grating [21]. For a single mode $n = 0$, the spoof surface mode is

$$\frac{w}{L_x}s_0^2\tan(kh) = \frac{\sqrt{k_x^2 - k^2}}{k} \tag{9}$$

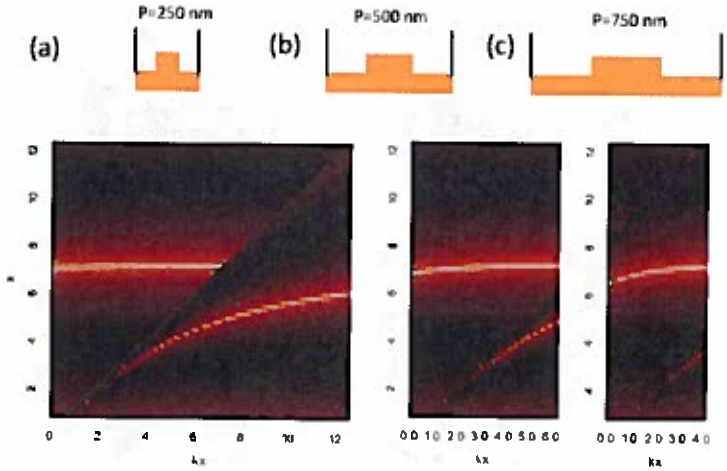

Fig. 2. Geometry induced surface plasmon mode dispersion as a function of the grating duty cycle. The grating period is L_x, the gap width w, and the grating depth, h. (a) Grating of $L_x = 250$nm with $w = 160$nm and depth,is fixed at $h = 216$nm. (b) Duty cycle 2, $L_x = 500$ nm and $w = 320$nm. (c) Duty cycle 3, $L_x = 750$ nm and $w = 480$nm.

which reduces to the standard result [5, 6].

Eq. (8) is a transcendental equation for the general dispersion of a resonant excitation of the perfect metallic grating. The solution of the transcendental equation for the resonance can be obtained graphically. The dispersion relationship is plotted graphically by considering

$$f(k,k_x) = \log\left|\frac{kw}{L_x}\sum_{n=-5}^{5}\frac{s_n^2}{\sqrt{k_x^{(n)2}-k^2}} - \cot(kh)\right|, \tag{10}$$

where the summation over n is cutoff. Fig. 2 shows the computed spoof plasmon dispersion relationship from a perfect conducting grating with the geometric dimensions outlined in the caption. In Figure 2, the grating duty cycle and depth are held fixed while the grating period is allowed to vary by the indicated multiplicative factors. The dispersion branches (bright lines) correspond to approximate solutions of the spoof plasmon resonance condition. The spoof surface mode dispersion lies below the lightline in Figure 2 and the flat dispersion to the left of the light line is due to band folding into the reduced Brillioun zone. The effective spoof surface plasmon wavelength for these geometric parameters can be obtained from the asymptotic k_x behavior. From Fig. 2, it is clear that the spoof mode dispersion is only weakly dependent on the period with fixed duty cycle and the effective plasmon wavelength is $\lambda_{pl} \approx 1140$ nm for the grating parameters in the caption. This should be contrasted with plasma wavelengths for real metals that occur in the ultraviolet portion of the spectrum. For instance, the Au plasma wavelength used in our Drude model is $\lambda_{pl} = 146$ nm in the UV part of the spectrum. The nature of the dispersive mode branch below the light line strongly confines the mode to the surface due to the exponential decay of the Bloch mode. The effect of nanostructure on the perfect conductor has created new dispersive surface modes which mimick surface plasmons with much lower plasma frequencies.

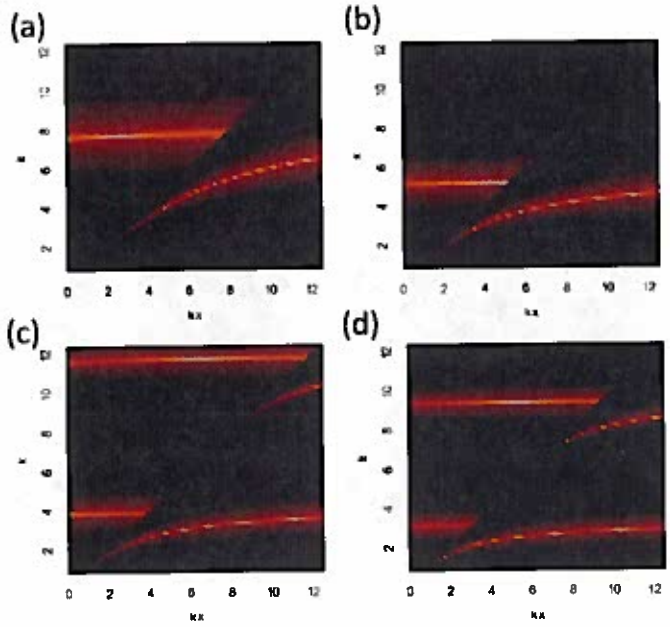

Fig. 3. Geometry induced surface plasmon mode dispersion versus the groove depth h. The grating period is 250 nm and the width 160 nm. (a) $h = 200$ nm. (b) $h = 300$ nm. (c) $h = 400$ nm. (d) $h = 500$ nm.

Figure 3 shows the influence of the grating depth on the geometrically induced surface mode for fixed period and duty cycle. Here the depth of grating is varied from 200 nm to 500 nm. The induced surface mode dispersion is seen to be very sensitive to grating depth, and becomes multimode at grating depths larger that 400 nm for the chosen period and duty cycle. Figure 4 shows the computed zeroth order reflection for p-polarized incident light using the Fourier modal scattering method (RCWA) from a Au grating using Drude model parameters for the permittivity. The Drude model permittivity is given by

$$\varepsilon(\omega) = 1 - \frac{\omega_{pl}^2}{\omega(\omega + i\gamma)}, \tag{11}$$

where $\omega_{pl} = 1.27524 \times 10^{16}$ sec^{-1}, and $\gamma = 6.59631 \times 10^{13}$ sec^{-1}. There is excellent correlation of the numerically computed modal dispersion for the finite conductive case with the analytic dispersion for the perfect conducting grating shown in figure 3 (c) for the same groove depth of 400 nm. The finite conductivity and the dispersion of the gratings permittivity only effects the values of the effective spoof plasmon dispersive resonances. This strong dependence of the spoof plasmon dispersion on the grating depth leads to an increased number of resonant surface modes of the grating and can be tailored by variation the geometric parameters of the grating. These spoof surface modes will be examined in the cavity configuration shown in figure 1 for finite conductive Au mirror and grating using the Drude permittivity. We will see that these spoof surface modes in periodically nanostructured cavities can have a large impact on cavity mode densities and subsequently a large impact on fluctuation induced forces at small mirror grating separations.

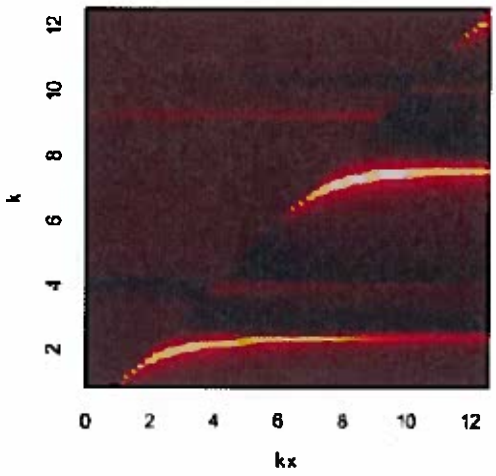

Fig. 4. Zeroth order TM polarized reflection $R_{0,0}$ from grating with finite conductivity given by the Drude model parameters for Au. The depth of the grating is $h = 400$ nm and the grating period is 250 nm.

3. Cavity Modes

In this section, we examine electromagnetic resonances in a planar periodically nanostructured cavity formed using real metallic mirrors and gratings. The cavity consists of a periodically structured grating below a planar mirror with a vacuum gap separating the two planar surfaces. Throughout, the mirrors are assumed to be Au and the metallic permittivity is treated by the Drude model [10]. Figure (1) illustrates the planar nanostructured cavity geometry under consideration. The modal properties in a planar periodic nanostructured cavity are obtained by Bloch modal expansion of the cavity fields in the three regions outlined in Fig. 1. The planar nature of the cavity mirrors and the underlying periodicity of the grating mirror implies that the modes are naturally expanded in a Bloch planewave mode basis. The cavity resonances are determined from the boundary conditions at the planar interfaces, and the eigenmode dispersion is obtained from the solution of the resulting secular equation. These resonant excitations are found to be cavity polaritons that result from the spoof surface modes induced within the cavity.

In general, the eigenmodes in the vacuum gap for the planar periodically nanostructured cavity are given by

$$\Psi_1(\mathbf{r},z) = \sum_{\nu} A_\nu X_{1\nu}^{(+)}(\mathbf{r}) \exp(ik\beta_\nu^{(+)} z) + B_\nu X_{1\nu}^{(-)}(\mathbf{r}) \exp(-ik\beta_\nu^{(-)} z), \tag{12}$$

where the coefficients A_ν and B_ν are determined by the scattering matrix method [10]. The modal solution is determined by splitting the cavity into three regions and requiring the continuity of the transverse fields across each of the planar interfaces. The cavity geometry in question consists of a planar mirror (surface 1) located at $z = -a$, and the periodically modulated grating substrate (surface 2) lies at $z = 0$. Explicitly, we define region 0 as a semi-infinite mirror region corresponding to surface 1, $-\infty < z \leq -a$; region 1 is the cavity vacuum gap between the the planar mirror and the planar top surface of the grating with $-a \leq z \leq 0$, and finally region 2, the etched grating region, $z \geq 0$. The transverse fields in each region can be

expanded in the eigenmodes, we have

$$\Psi_0 = \sum_\mu C_\mu X^{(-)}_{\mu,0} e^{-iq_z^{(0)}z} \tag{13}$$

$$\Psi_1 = \sum_\mu A_\mu X^{(+)}_{\mu,1} e^{iq_z^{(1)}z} + B_\mu X^{(-)}_{\mu,1} e^{-iq_z^{(1)}z} \tag{14}$$

$$\Psi_2 = \sum_\mu D_\mu X^{(+)}_{\mu,2} e^{iq_z^{(2)}z}. \tag{15}$$

where $q_z^{(i)} = \sqrt{k^2\varepsilon_i - q_n^2 - q_m^2}$ is the propagation eigenvalue for the uniform media in the ith region, and $\mu = (n,m,\sigma)$ where σ = s or p polarization. The boundary conditions on the continuity of the transverse fields at the two interfaces are $\Psi_0(z=-a) = \Psi_1(z=-a)$, and $\Psi_1(z=0) = \Psi_2(z=0)$. The simplest cavity that is amenable to an exact treatment is the cavity formed by two planar mirrors which forms a reference cavity with well defined cavity modes. The Bloch modes in this case reduce to planewave solutions for the uniform media and are derived in Eq. (49-52) for the eigenmodes.

In previous work, the Fourier modal solution to scattering from the periodically modulated surface using both S-matrix and T-matrix techniques has been described[10, 22, 23, 24, 25, 26]. Here, we will use the S-matrix formalism for scattering from the perioidically modulated surface to obtain a secular equation for the eigenmodes in the planar cavity. The boundary condition at the grating top surface ($z = 0$) is solved by the exact reflection matrix, R, which has been determined for arbitrary input amplitude A_μ. Eq. (14) can be rewritten as

$$\Psi_1 = \sum_\mu A_\nu \left(\delta_{\mu,\nu} X^{(+)}_{\mu,1} e^{iq_z^{(1)}z} + \sum_\nu R_{\mu,\nu} X^{(-)}_{\mu,1} e^{-iq_z^{(1)}z} \right). \tag{16}$$

where $B = RA$ in matrix notation (see Eq.(83) for the definition in terms of the S-matrix). The usage of the S-matrix implies that we have satisfied the continuity of the transverse field and scattering boundary conditions at $z = 0$. The boundary conditions at the planar mirror at $z = -a$ are the same as for the planar cavity case derived in the Appendix, and we obtain

$$C_\mu e^{iq_z^0 a} = i\alpha_\mu A_\mu e^{-iq_z^1 a} + \beta_\mu B_\mu e^{iq_z^1 a}, \tag{17}$$

where

$$\alpha_\mu = \begin{cases} \frac{1}{2\sqrt{q_z^{(0)} q_z^{(1)}}} (q_z^{(1)} - q_z^{(0)}) & \text{for s pol} \\ \frac{1}{2\sqrt{q_z^{(0)} q_z^{(1)}}} \left(\sqrt{\frac{\varepsilon_0}{\varepsilon_1}} q_z^{(1)} - \sqrt{\frac{\varepsilon_1}{\varepsilon_0}} q_z^{(0)} \right) & \text{for p pol.} \end{cases}$$

and

$$\beta_\mu = \begin{cases} \frac{1}{2\sqrt{q_z^{(0)} q_z^{(1)}}} (q_z^{(1)} + q_z^{(0)}) & \text{for s pol} \\ \frac{1}{2\sqrt{q_z^{(0)} q_z^{(1)}}} \left(\sqrt{\frac{\varepsilon_0}{\varepsilon_1}} q_z^{(1)} + \sqrt{\frac{\varepsilon_1}{\varepsilon_0}} q_z^{(0)} \right) & \text{for p pol.} \end{cases}$$

The z propagation terms, q_z, depend on the discrete spatial frequency index, $\mu = (nm, \sigma)$ and the polarization index σ =s or p. Furthermore, Eq. (59 -60) express the projection of the cavity mode onto the planar mirror mode and we obtain,

$$C_\mu = -\frac{i}{\alpha_\mu} A_\mu e^{-i(q_z^1 + q_z^0)a}. \tag{18}$$

The secular equation is

$$\sum_{\nu}\left(-i\delta_{\mu,\nu}\left(\frac{1}{\alpha_{\mu}}+\alpha_{\mu}\right)e^{-iq_{z}^{1}a}-e^{iq_{z}^{1}a}\beta_{\mu}R_{\mu,\nu}\right)A_{\nu}=0. \tag{19}$$

This can be simplified to give

$$\sum_{\nu}\left(\delta_{\mu,\nu}-e^{2iq_{z,\mu}^{(1)}a}\rho_{\mu}R_{\mu,\nu}\right)A_{\nu}=0, \tag{20}$$

where the cavity scattering matrix is defined as $\mathbf{D}_{\mu,\nu}=\delta_{\mu,\nu}-e^{2iq_{z,\mu}^{(1)}a}\rho_{\mu}R_{\mu,\nu}$, where

$$\rho_{\mu}=\begin{cases} ir_{s}^{nm}(1,0) & \text{for s pol} \\ ir_{p}^{nm}(1,0) & \text{for p pol,} \end{cases} \tag{21}$$

is the diagonal reflection matrix, and r_s and r_p are the Fresnel reflection coefficients from the planar interface. The generalized secular equation for the periodically modulated mirror cavity is now a matrix equation, and we require

$$\det(\mathbf{I}-e^{iq_{z}a}\cdot\rho\cdot e^{iq_{z}a}\cdot R)=0, \tag{22}$$

for non-trivial coefficients. Here $e^{iq_z a}$ are the diagonal propagation matrices. The solution to the general secular equation (Eq.(22)) for (ω,k_x,k_y) represent the dispersion relationships for the cavity resonances which depend parametrically on the mirror separation distance, a. In general, it may not be possible to find exact zeros for the secular equation for general complex scattering, and therefore we look to minimize the modulus of the secular determinant.

4. Results

The cavity dispersion can be examined graphically by plotting the secular determinant

$$|\log(\det(\mathbf{D}(k_x,k_y,\omega,a))|, \tag{23}$$

and is shown in figure (5) for various planar mirror spacings, a. This quantity is related to the modal density of states and the modal energy per unit area in the cavity as outlined in the previous section. The modes are shown as bright lines in Figure (5) with the grating cavity in the left panel and the planar metal cavity shown in the right panel for comparison. The series (a)-(f) shows the cavity dispersion comparison as a function of the mirror separation for the nanostructured grating cavity and the planar mirror cavity.

At small separations for the grating cavity, a cavity surface polariton mode is seen below the light line. (see fig. (5 (a)-(d)) The effective plasmon wavelength is taken as the asymptotic frequency for the cavity polariton mode below the light line with an effective plasma wavelength of ~ 1.5 microns. No corresponding low frequency dispersive mode exists for the planar cavity structure. This cavity polariton mode occurs in the Au grating for the p polarized mode and can be compared to the computed geometrically induced (spoof) surface plasmon mode in the perfect conductor, which occurs at an effective plasmon wavelength of ≈ 898 nm.

The grating cavity modes at small values of $k_x \approx 0$ in the dispersion diagrams show splitting due to polarization. The s and p polarized reflections from the grating are very different for the two polarizations and result in the dark splitting between the higher order modes. In the planar cavity, there is neglible dispersion splitting at small k_x since the reflection from a planar mirror is degenerate for s and p polarization. At larger k_x near the light line, the planar cavity

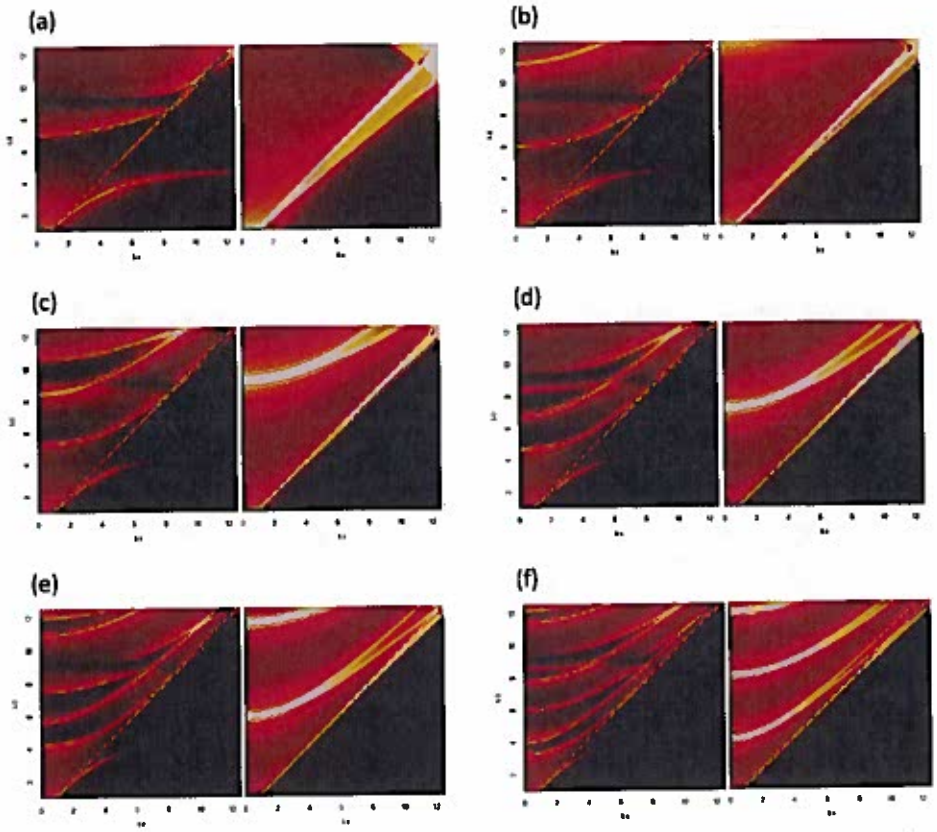

Fig. 5. Dispersion plots of nanostructure grating cavity (left panel) compared to plots of planar metallic mirror cavity. The plots are of $k_0 = \omega/c$ versus k_x for different separations. (a) $a = 100$ nm (b) $a = 200$ nm (c) $a = 300$ nm (d) $a = 400$ nm (e) $a = 500$ nm (f) $a = 750$ nm. The units of the k_0 and k_x are both in μm^{-1}.

modes are split due to small differences in large angle s and p polarized reflections from planar surfaces.

In the planar cavity at short mirror separations, we see a metal-vacuum-metal surface plasmon dispersion mode below the light line but asymptotically approaching the plasma frequency for Au, $k_{pl} = 2\pi/\lambda_{pl}$ with $\lambda_{pl} = 146$ nm. These well known surface plasmon modes occur in planar metallic cavities and waveguides at optical frequencies. In the grating cavity, the spoof surface mode changes the modal density of states at small mirror separation. As the separation is increased, we find that the modal density of states approaches the geometric or fill factor planar metal density of states.

At large mirror separations, we find that the cavity surface polariton mode disappears and that the dispersion consists of a series of mini-bands above the light line as in the metal-vacuum metal planar case. These mini-bands are split due to the polarized reflection of the grating but the overall modal number density is preserved. The large separation limit of the planar mirror cavity indicates that the p-polarized MIM gap mode dispersion can no longer be supported and merges with the light line mode from below.

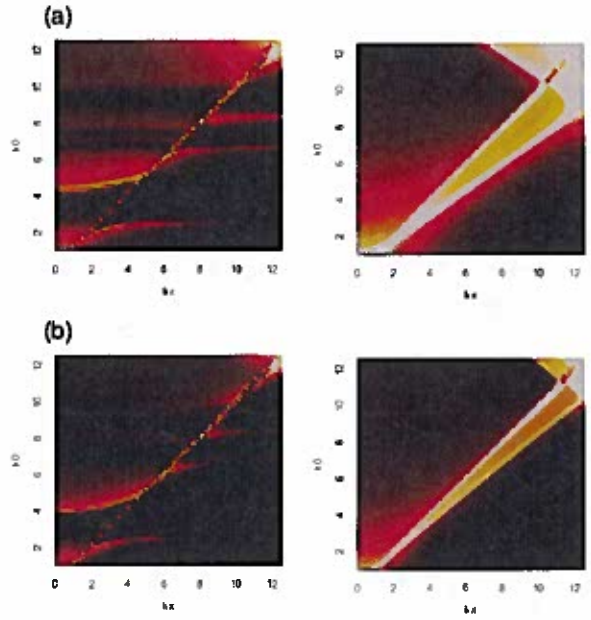

Fig. 6. Dispersion plots of nanostructure grating cavity (left panel) compared to plots of planar metallic mirror cavity. The plots are of $k_0 = \omega/c$ versus k_x for different separations. (a) $a = 50$ nm (b) $a = 100$ nm. The period is $L_x = 250$ nm, and the trench width, $w = 160$ nm same as Fig. (5), but the depth $h = 400$ nm. The units of the k_0 and k_x are both in μm^{-1}.

The impact of the grating depth is expected to have a large impact on the cavity polariton dispersion. Figure (6) shows the cavity dispersion for the same grating as in Fig. (5) but more deeply etched. Multimodal cavity surface polaritons are seen below the light line at very short mirror grating separation, $a = 50 - 100$ nm. This result is consistent with the prediction of multimodal spoof plasmon grating results shown in fig. (3) (d). The differences in the predicted effective plasma frequencies for each mode is attributed to the finite conductivity of the Au grating.

It is the geometrically induced cavity surface polariton mode from the nanostructured grating that alters the modal energy density in the nanostructured cavity at short separations. This can be seen since the modal density of states is proportional to the inverse of the $d\omega/dk_x$, which diverges at the Brillioun zone boundary for short separtions. This enhanced density of states leads to increased Casimir attraction at short separations, and the induced surface polariton mode creates a new effective length scale that is the induced or spoof surface mode plasmon wavelength. For the Au grating with the grating parameters used is approximately 1.5μm. Furthermore, the short distance enhancement and the asymptotic approach to the geometric PFA for the nanostructured grating cavity can be directly related to the presence and disappearance of the geometrically induced cavity surface polariton modes.

5. Conclusions

We have demonstrated that geometrically induced surface modes, or spoof plasmons, can have a dramatic impact on new hybridized cavity polariton modes in nanostructured cavities. These nanostructured cavities consist of a periodic grating and a planar mirror, which at short sepa-

rations exhibit dispersive cavity polaritonic resonances. These cavity polariton modes strongly confine light to the grating surface and can be designed to have dispersion in the infrared and THz regions of the spectrum. While these spoof surface modes are predicted for perfect conductive gratings, we have shown that these surface modes are also present on gratings with finite conductivity. Furthermore, the surface mode dispersion greatly effects the modal density of states in the cavity and enhances electromagnetic fluctuation driven forces and near field energy transfer at short mirror grating separations.

Although we have presented the cavity polaritons in a reflection based cavity, an analysis of a transmissive periodic nanostructured surface above a planar mirror or ground plane leads to similar resonant cavity modes. These modes can be coupled to by free space planewaves and lead to perfect absorbing structures. These perfect absorbers can have resonant modes in the infrared and have been observed in infrared frequency selective surfaces on a dielectric spacer above a ground plane[7]. It is expected that engineering the spoof surface plasmon dispersion can lead to a new class of energy harvesting devices based on these new infrared absorbing structures.

Acknowledgments

This research was funded by Sandia's Laboratory Directed Research and Development (LDRD) program. Sandia is a multiprogram laboratory operated by Sandia Corporation, a Lockheed Martin Company, for the United States Department of Energy's National Nuclear Security Administration under contract DE-AC04-94AL85000.

A. Modal Solution to Maxwells Equations

Fourier modal methods or planewave expansions are the method of choice in computing scattering from periodic media. These methods can be generalized to 3D periodic structures by considering decomposition of the complex dielectric permittivity into planar layers that are periodic in the transverse direction. Explicilty, this implies that

$$\varepsilon(\mathbf{x}) = \sum_{nm} \varepsilon_{nm}(z) \exp\left(i\frac{2\pi n}{L_x}x + i\frac{2\pi m}{L_y}y\right) \tag{24}$$

where $\varepsilon_{nm}(z)$ are the Fourier coefficients on a given layer. Likewise, it is clear that the transverse electric and magnetic fields must satisfy Floquet boundary conditions in each planar strate and are expanded into Bloch modes,

$$\vec{E}_t = e^{i\vec{k}\cdot\vec{r}} \sum_{nm} \vec{E}_{nm} \exp\left(i\frac{2\pi n}{L_x}x + i\frac{2\pi m}{L_y}y\right), \tag{25}$$

and

$$\vec{H}_t = e^{i\vec{k}\cdot\vec{r}} \sum_{nm} \vec{H}_{nm} \exp\left(i\frac{2\pi n}{L_x}x + i\frac{2\pi m}{L_y}y\right) \tag{26}$$

which satisfy the Bloch boundary conditions that arise due to the periodic nature of the permittivity and permeability. Here $\vec{E}_{nm}$ and $\vec{H}_{nm}$ are the Fourier coefficients of the transverse electric and magnetic fields, respectively. Similarly we expand the dielectric permittivity, magnetic permeability and their inverses in Fourier series. Substituting the Fourier expansions of the fields and the permittivity into the waveguide equations results in a complex first order matrix expression

$$-ik\partial_z \Psi_{n'm'} = \sum_{nm} \mathbf{H}_{n'm',nm} \Psi_{nm} \tag{27}$$

for the Fourier components of the complex electric and magnetic fields. The vector of the Fourier coefficients is

$$\Psi_{nm} = \begin{pmatrix} E^x_{nm} \\ E^y_{nm} \\ H^x_{nm} \\ H^y_{nm} \end{pmatrix}, \tag{28}$$

The complex matrix is given by

$$\mathbf{H}_{n'm';nm} = \begin{pmatrix} 0 & 0 & q_{n'}q_m\chi & -q_{n'}q_n\chi + k^2\delta \\ 0 & 0 & q_{m'}q_m\chi - k^2\delta & -q_nq_{m'}\chi \\ -q_{n'}q_m\delta & q_{n'}q_n\delta - k^2\varepsilon & 0 & 0 \\ -q_{m'}q_m\delta + k^2\varepsilon & q_nq_{m'}\delta & 0 & 0 \end{pmatrix}, \tag{29}$$

and where $\delta = \delta_{n,n'}\delta_{m,m'}$ is the product of kronecker delta functions, $\varepsilon = \varepsilon_{n'-n,m'-m}$, , and $\chi = (1/\varepsilon)_{n'-n,m'-m} = \chi_{n'-n,m'-m}$. These are the shifted Fourier expansions of the complex permittivity and its inverse. The Teoplitz structure of the permittivity has a consequences on the numerical solution . The eigenmodes in the 2D strata are obtained by considering H independent of the longitudinal coordinate z and by assuming a solution of the form

$$\Psi_{nm} = u_{nm}\exp(ik\beta z), \tag{30}$$

and substituting into Eq. (27), we obtain the eigenmode equation,

$$k^2\beta\, u_{n'm'} = \sum_{nm} \mathbf{H}_{n'm';nm}\, u_{nm}, \tag{31}$$

where β is the complex propagation constant. The propagation constants (β) are in general complex and the eigenvalues of the matrix H.

The left handed eigenvectors are the necessary compliment for guaranteeing the biorthogonality of the eigenmodes. The right and left eigenmodes are obtained from

$$\mathbf{H}\cdot u = k^2\beta u \tag{32}$$

$$v^T\cdot\mathbf{H} = k^2\beta v^T, \tag{33}$$

where v^T is the transpose of v. The mode orthogonality is

$$\sum_{nm} v^\nu_{nm}u^\mu_{nm} = \delta_{\mu,\nu}S_\nu, \tag{34}$$

where the normalization is

$$S_\mu = \sum_{nm} v^\mu_{nm}u^\mu_{nm}. \tag{35}$$

The orthogonality of the left handed and right handed eigenvectors can be directly related to the Poynting Reciprocity theorem as we demonstrated in the previous section. However, for non-uniform complex permittivity and permeability, Eq.(34) gives the general eigenvector biorthogonality relationship. In the following, we will consider the modes to be normalized resulting in orthonormality relationship

$$\sum_{nm} v^\nu_{nm}u^\mu_{nm} = \delta_{\nu,\mu}. \tag{36}$$

The transverse modal fields are given by

$$X_\nu(\mathbf{r}) = e^{i\vec{k}\cdot\vec{r}}\sum_{nm} u^\nu_{nm}\exp\left(i\frac{2\pi n}{L_x}x + i\frac{2\pi m}{L_y}y\right), \tag{37}$$

and we have a complementary expression for the left handed modal fields, $\tilde{X}^{\mu}(\vec{r})$,

$$\tilde{X}_{\nu}(\mathbf{r}) = e^{i\vec{k}\cdot\vec{r}} \sum_{nm} v_{nm}^{\nu *} \exp\left(i\frac{2\pi n}{L_x}x + i\frac{2\pi m}{L_y}y \right). \tag{38}$$

The transverse modal fields obey the orthogonality relationship,

$$\frac{1}{L_x L_y} \int \tilde{X}_{\mu}^{\dagger}(\mathbf{r}) X_{\nu}(\mathbf{r}) d\mathbf{r} = \delta_{\mu,\nu}. \tag{39}$$

where we have used explicitly the bi-orthogonality of u and $w^{\dagger}$.

The modal fields and their orthogonal compliment (right and left handed eigenmodes) from a complete basis on the 2D unit cell of the layer strata and can be used to expand an arbitrary field as a superposition of eigenmodes. The general transverse field expansion is

$$\Psi(\mathbf{r},z) = \sum_{\nu} C_{\nu} X_{\nu}(\mathbf{r}) \exp(ik\beta_{\nu} z), \tag{40}$$

where C_{ν} are the expansion coefficients, and β_{ν} are the complex propagation constants for the modes. The modal expansion of the transverse fields is a natural basis for scattering from structured lamellar strata since the boundary conditions on the continuity of the tangential fields are readily obtained. In the next section, the modal expansion will be used to develop an S-matrix scattering theory from our 2D periodic lamellar structure.

B. Uniform media: planewave modes

In a uniform medium, the permittivity and permeability are diagonal in fourier spatial frequencies, and Eq.(29) is a 4×4 matrix. The eigenvalue problem reduces to solutions of the secular equation

$$\det(\mathbf{H} - k^2\beta \mathbf{1}) = 0, \tag{41}$$

where the $\mathbf{H}$ matrix is diagonal, $\mathbf{H}_{n'm',nm} = \delta_{n,n'}\delta_{m,m'}\mathbf{H}_{nm}$ and is given by

$$\mathbf{H}_{nm} = \begin{pmatrix} 0 & 0 & q_n q_m/\varepsilon & (-q_n q_n + k^2\mu\varepsilon)/\varepsilon \\ 0 & 0 & (q_m q_m - k^2\mu\varepsilon)/\varepsilon & -q_n q_m/\varepsilon \\ -q_n q_m/\mu & (q_n q_n - k^2\varepsilon\mu)/\mu & 0 & 0 \\ (-q_m q_m + k^2\varepsilon\mu)/\mu & q_n q_m/\mu & 0 & 0 \end{pmatrix}. \tag{42}$$

The propagation eigenvalues in a uniform medium are

$$\beta_{nm} = \pm\sqrt{k^2\varepsilon\mu - q_n^2 - q_m^2}/k, \tag{43}$$

which is the normalized planewave wavevector for propagation in the z direction, and $q_n = k_x + \frac{2\pi n}{L_x}$ and $q_m = k_y + \frac{2\pi m}{L_y}$. The eigenmodes are the transverse components of a planewave and given by

$$u_{nm}^{(\pm)} = \frac{1}{k\mu} \begin{pmatrix} k\mu E_x^{\pm} \\ k\mu E_y^{\pm} \\ -\frac{\pm 1}{k\beta_{nm}}[(q_n q_m E_x^{\pm} + (k^2\varepsilon\mu - q_n^2)E_y^{\pm}] \\ \frac{\pm 1}{k\beta_{nm}}[(q_n q_m E_y^{\pm} + (k^2\varepsilon\mu - q_m^2)E_x^{\pm}] \end{pmatrix} \tag{44}$$

where $\pm$ refers to forward and backward propagating planewaves and $E_x^{\pm}$ and $E_y^{\pm}$ are determined by the normalization and orthogonality. Furthermore, we require that the eigenmodes are orthogonal for distinct eigenvalues.

We define the two orthogonal polarization (TE and TM) unit vectors as

$$\hat{e}_{TE} = \frac{\mathbf{q} \times \hat{e}_z}{\| \mathbf{q} \times \hat{e}_z \|} \tag{45}$$

$$\hat{e}^{\mu}_{TM} = \frac{\mathbf{q} \times \hat{e}_{TE}}{\| \mathbf{q} \times \hat{e}_{TE} \|}. \tag{46}$$

The coefficients depend explicitly on the propagating wavevector $\mathbf{q} = (\vec{q}, \mu q_z)$ and the angular frequency ω, but we will only include them explicitly for clarity. Furthermore, we will consider $\mu = 1$ and ε real throughout. The transverse components of the polarization unit vectors are

$$\hat{e}_s = \frac{1}{|\vec{q}|}(q_y \hat{e}_x - q_x \hat{e}_y) \tag{47}$$

$$\hat{e}_p = \frac{1}{|\vec{q}|}(q_x \hat{e}_x + q_y \hat{e}_y), \tag{48}$$

where $|\vec{q}|$ is the norm of transverse wavevector. We note that $\hat{e}_p \cdot \hat{e}_s = 0$. The resulting right handed eigenmode functions are

$$u^{(\pm)}_{nm,s} = \sqrt{\frac{\pm k}{2q_z}} \begin{pmatrix} \hat{e}_s \\ \pm \frac{q_z}{k} \hat{e}_p \end{pmatrix}. \tag{49}$$

and

$$u^{(\pm)}_{nm,p} = \sqrt{\frac{\pm k}{2q_z}} \begin{pmatrix} \pm \frac{q_z}{k\sqrt{\varepsilon}} \hat{e}_p \\ -\sqrt{\varepsilon} \hat{e}_s \end{pmatrix}, \tag{50}$$

and the left handed conjugate eigenmodes are

$$v^{(\pm)}_{nm,s} = \sqrt{\frac{\pm k}{2q_z}} \begin{pmatrix} \pm \frac{q_z}{k} \hat{e}_s \\ \hat{e}_p \end{pmatrix}, \tag{51}$$

and

$$v^{(\pm)}_{nm,p} = \sqrt{\frac{\pm k}{2q_z}} \begin{pmatrix} \sqrt{\varepsilon} \hat{e}_p \\ \mp \frac{q_z}{k\sqrt{\varepsilon}} \hat{e}_s \end{pmatrix}. \tag{52}$$

These eigenmodes are by construction orthogonal and can be normalized to form an orthonormal planewave basis. The case of normal incidence requires special care since the plane of incidence is not defined. The orthonormal basis can be constructed by taking the limit of vanishing transverse spatial frequencies in a fixed order, say $q_x \to 0$ before $q_y \to 0$.

C. Planar Mirror Cavity

By utilizing the mode orthonormality for the eigenmodes in media 2, and media 0, we obtain

$$D_s = \frac{1}{2\sqrt{q_z^{(2)} q_z^{(1)}}} \left(A_s (q_z^{(2)} + q_z^{(1)}) + i B_s (q_z^{(2)} - q_z^{(1)}) \right) \tag{53}$$

$$D_p = \frac{1}{2\sqrt{q_z^{(2)} q_z^{(1)}}} \left[A_p \left(\sqrt{\frac{\varepsilon_1}{\varepsilon_2}} q_z^{(2)} + \sqrt{\frac{\varepsilon_2}{\varepsilon_1}} q_z^{(1)} \right) + i B_p \left(\sqrt{\frac{\varepsilon_1}{\varepsilon_2}} q_z^{(2)} - \sqrt{\frac{\varepsilon_2}{\varepsilon_1}} q_z^{(1)} \right) \right] \tag{54}$$

for s and p polarizations at $z = 0$, and

$$C_s e^{iq_z^0 a} = \frac{1}{2\sqrt{q_z^{(0)} q_z^{(1)}}} \left(iA_s e^{-iq_z^1 a}(q_z^{(1)} - q_z^{(0)}) + B_s e^{iq_z^1 a}(q_z^{(1)} + q_z^{(0)}) \right) \tag{55}$$

$$C_p e^{iq_z^0 a} = \frac{1}{2\sqrt{q_z^{(0)} q_z^{(1)}}} \left[iA_p e^{-iq_z^1 a} \left(\sqrt{\frac{\varepsilon_0}{\varepsilon_1}} q_z^{(1)} - \sqrt{\frac{\varepsilon_1}{\varepsilon_0}} q_z^{(0)} \right) \right. \tag{56}$$

$$\left. + B_p e^{iq_z^1 a} \left(\sqrt{\frac{\varepsilon_0}{\varepsilon_1}} q_z^{(1)} + \sqrt{\frac{\varepsilon_1}{\varepsilon_0}} q_z^{(0)} \right) \right],$$

at $z = -a$ by projection. Alternatively, we can directly compute the transmission by projection at z=0 ,

$$D_s = \frac{2\sqrt{q_z^{(2)} q_z^{(1)}}}{(q_z^{(2)} + q_z^{(1)})} A_s \tag{57}$$

$$D_p = \frac{2\sqrt{q_z^{(2)} q_z^{(1)}}}{\sqrt{\frac{\varepsilon_1}{\varepsilon_2}} q_z^{(2)} + \sqrt{\frac{\varepsilon_2}{\varepsilon_1}} q_z^{(1)}} A_p, \tag{58}$$

and at $z = -a$

$$C_s = -i \frac{2\sqrt{q_z^{(0)} q_z^{(1)}}}{(q_z^{(1)} - q_z^{(0)})} A_s e^{-i(q_z^1 + q_z^0)a} \tag{59}$$

$$C_p = -i \frac{2\sqrt{q_z^{(0)} q_z^{(1)}}}{\left(\sqrt{\frac{\varepsilon_0}{\varepsilon_1}} q_z^{(1)} - \sqrt{\frac{\varepsilon_1}{\varepsilon_0}} q_z^{(0)} \right)} A_p e^{-i(q_z^1 + q_z^0)a}. \tag{60}$$

for s and p polarizations.

Our goal is to obtain a secular type equation describing modes in the cavity. This can be accomplished by substitution of the transmission expressions into Eq.(53-54) or equivalently Eq.(55-56) and equating A and B coefficients. We start at $z = 0$, and obtain reflection coefficients

$$iB_s = \left(\frac{q_z^{(1)} - q_z^{(2)}}{q_z^{(1)} + q_z^{(2)}} \right) A_s \tag{61}$$

$$iB_p = \left(\frac{\sqrt{\frac{\varepsilon_2}{\varepsilon_1}} q_z^{(1)} - \sqrt{\frac{\varepsilon_1}{\varepsilon_2}} q_z^{(2)}}{\sqrt{\frac{\varepsilon_2}{\varepsilon_1}} q_z^{(1)} + \sqrt{\frac{\varepsilon_1}{\varepsilon_2}} q_z^{(2)}} \right) A_p. \tag{62}$$

We have utilized the $z = 0$ solution, Eq. (53-54), to relate the eigenmode expansion coefficients in the cavity between the two planar mirrors. The cavity modal solution or secular equation further requires that the solution to Eq.(55-56) at $z = -a$. The secular equation is obtained by substitution and we obtain

$$\left[1 - \left(\frac{q_z^{(1)} - q_z^{(2)}}{q_z^{(1)} + q_z^{(2)}} \right) \left(\frac{q_z^{(1)} - q_z^{(0)}}{q_z^{(1)} + q_z^{(0)}} \right) e^{2iq_z^{(1)} a} \right] A_s = 0 \tag{63}$$

$$\left[1 - \left(\frac{\sqrt{\frac{\varepsilon_2}{\varepsilon_1}} q_z^{(1)} - \sqrt{\frac{\varepsilon_1}{\varepsilon_2}} q_z^{(2)}}{\sqrt{\frac{\varepsilon_2}{\varepsilon_1}} q_z^{(1)} + \sqrt{\frac{\varepsilon_1}{\varepsilon_2}} q_z^{(2)}} \right) \left(\frac{\sqrt{\frac{\varepsilon_0}{\varepsilon_1}} q_z^{(1)} - \sqrt{\frac{\varepsilon_1}{\varepsilon_0}} q_z^{(0)}}{\sqrt{\frac{\varepsilon_0}{\varepsilon_1}} q_z^{(1)} + \sqrt{\frac{\varepsilon_1}{\varepsilon_0}} q_z^{(0)}} \right) e^{2iq_z^{(1)} a} \right] A_p = 0. \tag{64}$$

It is convenient to introduce the generalized reflection coefficients

$$r_s(i,j) = \left(\frac{q_z^{(i)} - q_z^{(j)}}{q_z^{(i)} + q_z^{(j)}}\right) \tag{65}$$

$$r_p(i,j) = \left(\frac{\sqrt{\frac{\varepsilon_j}{\varepsilon_i}} q_z^{(i)} - \sqrt{\frac{\varepsilon_i}{\varepsilon_j}} q_z^{(j)}}{\sqrt{\frac{\varepsilon_j}{\varepsilon_i}} q_z^{(i)} + \sqrt{\frac{\varepsilon_i}{\varepsilon_j}} q_z^{(j)}}\right) \tag{66}$$

The cavity eigenmodes are non-trivial solutions of the above equations for the propagation constants or eigenfrequencies. The secular equation for the modes in the cavity becomes,

$$1 = r_s(1,2) r_s(1,0) e^{2iq_z^{(1)}a} \tag{67}$$

$$1 = r_p(1,2) r_p(1,0) e^{2iq_z^{(1)}a}. \tag{68}$$

The secular equation defines two transcendental equations, one for each polarization whose solution gives the modal dispersion in the planar cavity. The interpretation of the secular equations is quite simple. It represents the in-phase round trip scattering in the cavity, where the reflection coefficients are from the two planar mirrors, and the complex phase is the Rayleigh propagation factor for the round trip.

The solution of the secular equation for each polarization corresponds to the dispersion, $(\omega, \vec{k}_t)$, for a resonance or propagating mode in the cavity. Indeed, this form of the secular equations are a ray-optics resonance condition for waveguiding in a dielectric slab waveguide [Chuang]. Furthermore, the p polarized secular equation can be further reduced to give

$$(\varepsilon_2 q_z^{(1)} + \varepsilon_1 q_z^{(2)})(\varepsilon_0 q_z^{(1)} + \varepsilon_1 q_z^{(0)}) = (\varepsilon_2 q_z^{(1)} - \varepsilon_1 q_z^{(2)})(\varepsilon_0 q_z^{(1)} - \varepsilon_1 q_z^{(0)}) e^{2iq_z^{(1)}a}, \tag{69}$$

which is the resonance condition for surface plasmon modes in metal-insulator-metal or insulator-metal-insulator waveguiding structures. [Raether]

D. Scattering

We now consider the eigenmode expansion and its use in EM scattering problems in planar stacks. Fig. (1) b) shows schematically the layered strata of 2D periodic scatterers. The incident media (0th layer) and the exit media (N+1th) are assumed to be uniform layers with planewave type eigenmodes. In each layer, the tangential fields are represented as an eigenmode expansion and can be split into forward and backward propagating modes given by,

$$\Psi^i(\vec{r},z) = \sum_\nu A_\nu^i X_{i,\nu}^{(+)}(\vec{r}) \exp(ik\beta_{i,\nu}^{(+)} z) + B_\nu^i X_{i,\nu}^{(-)}(\vec{r}) \exp(-ik\beta_{i,\nu}^{(-)} z), \tag{70}$$

which completely determine the electromagnetic field in the i layer. Here, $X^{\pm}(\mathbf{r})$ and $\beta^{\pm}$ are the forward and backward transverse mode functions and progation constants respectively. For a scattering calculation, we have

$$\Psi^0(\vec{r},z) = \Psi^{inc}(\vec{r},z) + \Psi^{scattered}(\vec{r},z), \tag{71}$$

where the incident mode coefficients, $A_{\nu_k}^0$ are input to the calculation. The determination of the mode coefficients in the incident and exit media constitutes a solution to the scattering problem.

D.0.1. Transfer Matrix

From the boundary conditions on the continuity of the tangential fields at the ith interface, we define the interface transfer matrix,

$$\begin{pmatrix} A_{i+1} \\ B_{i+1} \end{pmatrix} = \begin{pmatrix} t_{11}\exp(i\gamma^{+}) & t_{12}\exp(i\gamma^{-}) \\ t_{21}\exp(i\gamma^{+}) & t_{22}\exp(i\gamma^{-}) \end{pmatrix} \begin{pmatrix} A_i \\ B_i \end{pmatrix} \tag{72}$$

which relates the coefficients in the ith to i+1th media and $\gamma^{(\pm)} = \pm k\beta^{(\pm)} \cdot d_i$, and $d_i = z_i - z_{i-1}$ is the thickness of the ith layer. Here each layer transfer matrix can be expressed in terms of the layer overlaps of the mode eigenvectors and is given by

$$\begin{aligned} t_{11} &= \sum_{nm} v_{nm}^{\nu(+)}(i+1)u_{nm}^{\mu(+)}(i) \\ t_{12} &= \sum_{nm} v_{nm}^{\nu(+)}(i+1)u_{nm}^{\mu(-)}(i) \\ t_{21} &= \sum_{nm} v_{nm}^{\nu(-)}(i+1)u_{nm}^{\mu(+)}(i) \\ t_{22} &= \sum_{nm} v_{nm}^{\nu(-)}(i+1)u_{nm}^{\mu(-)}(i) \end{aligned} \tag{73}$$

where we sum over the Fourier coefficients for the eigenvectors.

The transfer matrix can be iterated through the planar structure to obtain the global transfer matrix

$$T_{\nu,\mu} = \sum_{\mu_N} \cdots \sum_{\mu_1} T_{\nu,\mu_N}^{N+1,N} T_{\mu_N,\mu_{N-1}}^{N,N-1} \cdots T_{\mu_1,\mu}^{1,0}, \tag{74}$$

which connects the incident and reflected mode coefficients to the transmitted mode coefficients. The global transfer matrix is the product of the individual layer transfer matrices and is given by

$$\begin{pmatrix} A_{N+1} \\ B_{N+1} \end{pmatrix} = \begin{pmatrix} T_{11} & T_{12} \\ T_{21} & T_{22} \end{pmatrix} \cdot \begin{pmatrix} A_0 \\ B_0 \end{pmatrix}. \tag{75}$$

We can solve for the reflection and transmission mode coefficients where

$$\begin{aligned} B_0 &= -T_{22}^{-1} \cdot T_{21} \cdot A_0 \\ A_{N+1} &= (T_{11} - T_{12} \cdot T_{22}^{-1} \cdot T_{21}) \cdot A_0. \end{aligned} \tag{76}$$

Here A_{N+1} is the transmission and B_0 is the reflection coefficient vectors . We can define the reflection matrix, $R = -T_{22}^{-1} \cdot T_{21}$ and the transmission matrix $T = T_{11} + T_{12} \cdot R$.

D.0.2. S matrix

The transfer matrix product is known to suffer from instabilities when the layers are thick. A remedy to the numerical instabilities is the S-matrix approach. The S-matrix approach is derived from the ordered T-matrix, where the ordering is in terms of forward and back propagating modes. The S-matrix can be defined by reordering the coefficients and can be expressed in terms of the interface transfer matrices,

$$\begin{pmatrix} A_{i+1} \\ B_i \end{pmatrix} = \begin{pmatrix} 1 & 0 \\ 0 & \exp(-i\gamma^{-}) \end{pmatrix} \begin{pmatrix} \sigma_{11} & \sigma_{12} \\ \sigma_{21} & \sigma_{22} \end{pmatrix} \begin{pmatrix} \exp(i\gamma^{+}) & 0 \\ 0 & 1 \end{pmatrix} \cdot \begin{pmatrix} A_i \\ B_{i+1} \end{pmatrix} \tag{77}$$

where the interface s-matrix is

$$\begin{pmatrix} \sigma_{11} & \sigma_{12} \\ \sigma_{21} & \sigma_{22} \end{pmatrix} = \begin{pmatrix} t_{11} - t_{12}t_{22}^{-1}t_{21} & t_{12}t_{22}^{-1} \\ -t_{22}^{-1}t_{21} & t_{22}^{-1} \end{pmatrix}. \tag{78}$$

The S-matrix stability is guaranteed in Eq. (78) due to the exponential decay of the backward propagating mode . The layer S-matrix incorporates the propagation phase factor and the interface S-matrices and is given by

$$\begin{pmatrix} A_{i+1} \\ B_i \end{pmatrix} = \begin{pmatrix} s_{11}^i & s_{12}^i \\ s_{21}^i & s_{22}^i \end{pmatrix} \cdot \begin{pmatrix} A_i \\ B_{i+1} \end{pmatrix}. \tag{79}$$

We therefore have an iterative procedure to construct the global S matrix which

$$\begin{pmatrix} A_{N+1} \\ B_0 \end{pmatrix} = \begin{pmatrix} S_{11}^{(N)} & S_{12}^{(N)} \\ S_{21}^{(N)} & S_{22}^{(N)} \end{pmatrix} \cdot \begin{pmatrix} A_0 \\ B_{N+1} \end{pmatrix} \tag{80}$$

which connects the incident media (incident and reflected modes) to the exit media (transmitted modes). The recursion relations for the S-matrix are

$$\begin{aligned} S_{11}^{(i)} &= s_{11}^i \left(1 - S_{12}^{(i-1)} s_{21}^i\right)^{-1} S_{11}^{(i-1)} \\ S_{12}^{(i)} &= s_{12}^i + s_{11}^i \left(1 - S_{12}^{(i-1)} s_{21}^i\right)^{-1} S_{12}^{(i-1)} s_{22}^i \\ S_{21}^{(i)} &= S_{21}^{(i-1)} + S_{22}^{(i-1)} \left(1 - s_{21}^i S_{12}^{(i-1)}\right)^{-1} s_{21}^i S_{11}^{(i-1)} \\ S_{22}^{(i)} &= S_{22}^{(i-1)} \left(1 - s_{21}^i S_{12}^{(i-1)}\right)^{-1} s_{22}^i \end{aligned} \tag{81}$$

where the initial S-matrix iterates are the layer s-matrices in the incident media. The transmitted mode coefficients are given by

$$A_{N+1} = S_{11} A_0 \tag{82}$$

and the reflected mode coeffients are

$$B_0 = S_{21} A_0. \tag{83}$$

The transmitted and reflected diffraction orders are obtained from the mode coefficients and the Fourier eigenmodes in the incident and transmitted media. The resulting reflection and transmission matrices are

$$R = S_{21} \tag{84}$$

$$T = S_{11} \tag{85}$$

which are directly related to the S-matrix elements. The S-matrix completely determines the scattering amplitudes and plays a critical role in planar cavity multiple scattering.